ISPRS Journal of Photogrammetry and Remote Sensing 117 (2016) 161–171

Contents lists available at ScienceDirect

ISPRS Journal of Photogrammetry and Remote Sensing

journal homepage: www.elsevier.com/locate/isprsjprs

A general variational framework considering cast shadows for the topographic correction of remote sensing imagery

Huifang Li [a,b], Liming Xu [c], Huanfeng Shen [a,d,*], Liangpei Zhang [d,e]

[a] School of Resource and Environmental Sciences, Wuhan University, PR China
[b] Key Laboratory of Geographic Information System, Ministry of Education, Wuhan, PR China
[c] Hangzhou Dingchuan Information Technology Co. Ltd., Zhejiang Province, PR China
[d] Collaborative Innovation Center of Geospatial Technology, Wuhan, PR China
[e] The State Key Laboratory of Information Engineering in Surveying, Mapping and Remote Sensing, Wuhan University, PR China

ARTICLE INFO

Article history:
Received 19 November 2015
Received in revised form 16 March 2016
Accepted 31 March 2016
Available online 23 April 2016

Keywords:
Topographic correction
Cast shadow
Variational framework

ABSTRACT

Topographic shadows are inevitable obstacles for the interpretation of remote sensing images covering rugged terrain. A general variational topographic correction (TC) framework is proposed in this paper by considering not only self shadows but also cast shadows. Cast shadows are first detected by integrating the radiometric and topographic features of the observed region. The cosine values of the incidence angles for the cast shadows are then corrected by the variational framework. The corrected incidence angles can be used in any traditional TC model to compensate for the shadows in mountainous regions. The proposed variational framework was utilized in eight different traditional TC models, and the results were compared with the traditional results. Images from two different regions were employed to test the framework. The results suggest that the proposed framework can raise the accuracy of shadow correction by both subjective and objective evaluations, owing to the correction of the cast shadows.

1. Introduction

Great parts of the earth's surface are covered by rugged terrain, in which mountains and valleys are widely spread. The variation of the elevation affects the distribution of the sun's radiation, causing sunlit and shaded areas, which correspond to the bright and dark pixels in remotely sensed imagery (Sandmeier and Itten, 1997). As a result of the lack of radiation in shaded areas, the information in shaded pixels is less than that in sunlit pixels. This is the reason why it is difficult to interpret remotely sensed data of mountainous areas. Topographic correction (TC) aims to compensate for the lost radiation for shaded pixels in remotely sensed imagery, which can help to raise the quality and applicability of images covering mountainous terrain (Smith et al., 1980). Thus, TC is usually considered as an important step before remote sensing imagery is used in many applications (Richter et al., 2009; Vanonckelen et al., 2013).

The current TC methods can be divided into two types: physical model based methods and data-based empirical methods. The former type depends on the radiative transfer model, considering both the atmospheric and topographic conditions (Balthazar et al., 2012; Dymond et al., 2001; Richter, 1996). The physical model based methods require in-situ atmospheric parameters, which are often unavailable (Ghasemi et al., 2013; Proy et al., 1989). These methods are physically accurate, but are complicated and not widely used. The latter type is based on the topographic features and statistical information of the observed images (Civco, 1989; Teillet et al., 1982). These data-based empirical methods are simple and general approaches that can be used with most remote sensing data (Ge et al., 2008; Minnaert, 1941). In this paper, we concentrate on the latter type of TC method, and we attempt to make some improvements by constructing a general variational framework.

According to the geometric relationship between the sun and the earth, shaded pixels locate in two different regions: the shady slopes of mountains and the shadows of mountains cast on adjacent regions, corresponding to self shadow and cast shadow (Funka-Lea and Bajcsy, 1995; Teillet et al., 1997; Li et al., 2014). This paper focuses on the cast shadow and the specific definitions of self and cast shadow are given in Section 2. The topographic features used in the current methods are extracted from the digital elevation model (DEM) data, which describe the elevation, slope, and the aspect of the land surface (Riaño et al., 2003). The

* Corresponding author at: School of Resource and Environmental Sciences, Wuhan University, PR China.

http://dx.doi.org/10.1016/j.isprsjprs.2016.03.021
0924-2716/

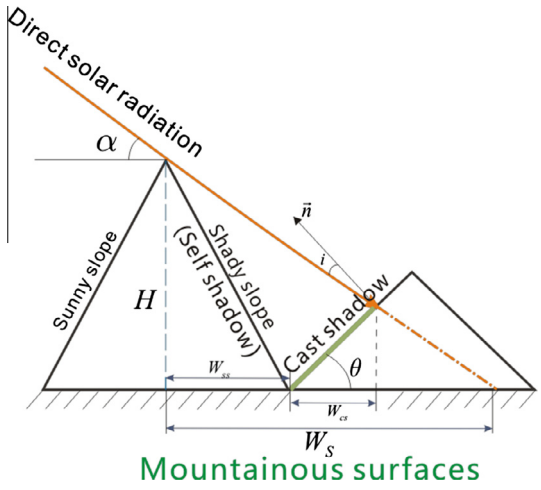

Fig. 1. The full shadow, including the self shadow and cast shadow, where the incident angle i is the angle between the solar radiation vector and the normal vector of the surface ($\vec{n}$).

correction is based on one important topographic feature: the cosine of the solar incidence angle ($\cos i$) of the land surface, as shown in Fig. 1, which is calculated by considering the solar position, the slope, and the aspect of the surface. The $\cos i$ is small for shaded slopes, and large for sunlit slopes. Thus, shaded slopes can be corrected by the current TC methods. However, the cast shadows actually locate on sunlit slopes. The current TC methods only consider the radiometric distortion caused by the self shadows, and overlook the adjacent cast shadows (Gao and Zhang, 2009; Kobayashi and Sanga Ngoie, 2008; Meyer et al., 1993). This is the reason why some dark regions often still exist in the correction results adjacent to self shadows (Kobayashi and Sanga Ngoie, 2009).

We attempt here to propose a TC method that can correct all the radiometric distortion caused by shadows, including both self shadows and cast shadows in remote sensing images with medium spatial resolutions. The cast shadow range and its influences are first discussed in detail. The topographic features and the radiometric information are then combined to distinguish between self shadows and cast shadows. Finally, a variational framework is constructed to optimize the topographic features by treating the self and cast shadows differently. This variational framework can be generally applied to all the current TC models, and is effective in correcting cast shadows.

The rest of the paper is organized as follows. The shadow components are analyzed in details and three traditional TC models are reviewed in Section 2. The proposed method is described in Section 3, including cast shadow detection, the variational framework, and its application. The experiments and results are described in Section 4. Finally, the paper is concluded in Section 5.

2. Problem analysis for topographic correction (TC)

Topographic correction has been studied by many researchers and some classical TC models have been proposed and improved. The shadow components and their effects on TC are analyzed in details, and meanwhile three traditional TC models are reviewed.

2.1. Shadow components: self shadows and cast shadows

Shadows refer to regions lacking direct solar illumination, which can be attributed to two reasons: opposing the sun and cast by obstructions. As shown in Fig. 1, the light source locates on the upper left of the 2D space. The shady slope opposes the sun, causing the self shadow, while the cast shadow is caused by the obstruction of the neighbor peak, even though it locates on a sunlit slope. An important criterion to distinguish self shadow and cast shadow is whether there is free space between where the shadow is and where the obstruction is (Funka-Lea and Bajcsy, 1995). If the free space exists, it is the cast shadow, otherwise it is the self shadow. It is noted that the mount is constituted by a lot of peaks, which are adjacent, convex and independent objects. They can cast shadows on the neighborhoods rather than themselves along the incident direction of the sun. We focus on processing the cast shadow in the topographic correction which is neglected in the traditional models.

How large are cast shadows, and can they be neglected in a remote sensing image? Assuming that the sun elevation is α and the height of the mountain is H, then the shadow width W_S can be calculated by the following equation:

$$W_S = H/\tan(\alpha) \tag{1}$$

The width of the self shadow W_{ss} is equal to the half width of the mountain, which is included in the total shadow W_S. The cast shadow width W_{cs} can then be calculated by the sine theorem, i.e.

$$W_{cs} = \cos\theta \sin\alpha(W_S - W_{ss})/\sin(\alpha+\theta) \tag{2}$$

where θ is the slope of the adjacent surface. W_{cs} is negatively related to the slope of the adjacent surface, which means that the smaller the value of θ, the larger the value of W_{cs}. Assuming $\alpha = 35°$, $H = 1000$ m, $W_{ss} = 500$ m, and $\theta = 40°$, the cast shadow width can be calculated as $W_{cs} = 422.2$ m. This cast shadow would cover more than 10 pixels in an image with a 30-m spatial resolution. If a TC method only treats self shadows, the correction will not be complete because the radiometric distortion caused by cast shadows will still exist in the image. Thus, cast shadows cannot be neglected in TC. The self shadow plus the cast shadow comprises the full shadow.

Pixels covered by shadows, either self shadows or cast shadows, are dark with a low radiance. The difference is that the incidence angles of self-shadow pixels are large, but they are small for the cast shadows. This means that the $\cos i$ of self shadows is small, and the $\cos i$ of cast shadows is large. For sunlit pixels, the $\cos i$ is large, as well as the radiance. Therefore, a positive linear relationship between $\cos i$ and the radiance holds for the sunlit and self shadow pixels, which can be expressed as:

$$L_T = a + b\cos i \tag{3}$$

where L_T is the observed radiation, $\cos i$ is the cosine of the incidence angle, b is the slope of the regression line, and a is the intercept. The same symbols represent the same variables in this paper. However, the cast shadows violate this relationship. Most of the traditional TC models are constructed based on this linear relationship. Thus they cannot be used to correct the radiometric distortion of cast shadows. That is the reason why we especially consider cast shadows in our work. Before illustrating the proposed framework, three traditional TC models are first reviewed in the following.

2.2. Traditional TC methods

A number of traditional empirical TC methods are currently used, among which three widely used methods are reviewed and compared in this paper: the C-correction model (Teillet et al., 1982; Hantson and Chuvieco, 2011), the sun–canopy–sensor (SCS) correction model (Gu and Gillespie, 1998; Soenen et al., 2005; Fan et al., 2014), and statistical empirical correction (SEC) (McDonald et al., 2002). These models aim to remove the effects of rough terrain on the radiation, and obtain the radiation L_H under the supposing condition that the terrain is horizontal.

2.2.1. The C-correction model

Based on the linear relationship in Eq. (3), the sun incidence angle i equals to the sun zenith anglesz when the land surface is totally horizontal, i.e. $L_H = a + b\cos(sz)$, where L_H represents the radiation on a horizontal surface. Then the corrected radiance can be got by the following formula:

$$L_H = L_T \frac{\cos(sz) + c}{\cos i + c} \tag{4}$$

where c is the ratio of a and b, which can be expressed as $c = a/b$. a and b are estimated by linear regression based on samples extracted from the image.

2.2.2. The SCS correction model

Considering the roughness of the topographical surface, the sun–canopy–sensor model was proposed, in which the slope angle of the terrain was involved. Combining the advantage of C-correction, the improved SCS model can be expressed as:

$$L_H = L_T \frac{\cos(sz)\cos\alpha + c}{\cos i + c} \tag{5}$$

where α is the slope angle of each pixel, and c is obtained by the same way as it is in the C-correction model.

2.2.3. The SEC correction model

The SEC correction is a totally statistical information based model supposing the mean values of the horizontal surface and the tilted surface are equal. The correction function can be expressed as:

$$L_H = L_T - (b\cos i + a) + \bar{L}_T \tag{6}$$

where $\bar{L}_T$ is the mean radiance of the original rough terrain, a and b can be obtained by the same way as C and SCS correction models do.

Overall, these three traditional models are all constructed on the basic assumption of a linear relationship between the radiation and the sun incidence angles. All pixels are treated in the same way. Shadows are not categorized and cast shadows are not specifically considered.

3. The topographic correction (TC) method considering cast shadows

Considering the formation difference of self shadows and cast shadows, they are first separated and then optimized by different strategies before being used in the TC models. Thus, the proposed method is composed of three steps: (a) detect all the shadows and distinguish self shadows and cast shadows; (b) optimize the topographic features by a variational framework; and (c) apply the optimized topographic features in different TC models. The input data are the top of atmosphere (TOA) radiance of Landsat data.

3.1. Shadow detection

As mentioned in Section 3, shadows are composed of self shadows and cast shadows. They both appear dark in the imagery, but locate on totally opposite slopes. In this paper, the radiometric and topographic features are integrated to detect shadows in the remote sensing images. Thus, the shadow detection process is composed of two passes: full shadow and self shadow detection. The full shadow can be detected based on the radiometric and geometric information, which may introduce commission and omission errors (Corripio, 2003; Funka-Lea and Bajcsy, 1995). In this paper, the first pass is based on the radiometric information, for which the shadow index is constructed. The second pass is based on the topographic features, which are used to extract the self shadows. The cast shadows are finally detected by subtracting the self shadows from the full shadows. It should be noted that water is screened out before the TC.

3.1.1. The first pass: full shadow detection

In the radiometric feature aspect, shadows have obviously smaller radiances than most of the sunlit regions. On the other hand, with the increase in the wavelength, shadows become darker and darker due to the decrease in the atmospheric scattering radiance (Kaufman, 1984). For multispectral data including visible and infrared bands, the wavelength of blue is the shortest and the atmospheric scattering effect is the strongest, which causes the largest ambient irradiance in the blue band. This is why the same shadow area is brighter in the blue band than in all other bands. In contrast, in the near-infrared channels, the atmospheric scattering is minimal. However, the atmospheric scattering effect is equal for all objects in the same channel. The radiometric properties of different land-cover types should also be considered. The major land-cover type in mountainous regions is green vegetation, which has an obviously high reflectance in the near-infrared channel. Therefore, the radiance of the blue and near-infrared channels are used to extract shadows.

Based on the above two properties of shadows, we propose a shadow index (SI) to enhance shadows and suppress non-shadows. For multispectral remote sensing data, the SI can be expressed as the following function:

$$\mathrm{SI} = \frac{L_{blue} - L_{nir}}{(L_{blue} + L_{nir})L_{mean}} \tag{7}$$

where L_{blue} and L_{nir} represent the radiance of the blue and near-infrared channels, respectively, and L_{mean} is the mean of the radiance or reflectance of all reflective bands.

In a remote sensing image, the SI ranges from -1 to 1, i.e. high for shadows and low for sunlit areas. For vegetation in sunlit areas, the SI is negative. It should be noted that except water, some other dark objects such as tar/bitumen roads may also show high SI, which introduces commission error in the shadow detection result. These dark objects should be discriminated first and screened out from the shadow detection process. The major dark object in the mountainous image with medium spatial resolutions is water, which is actually horizontal and should be excluded from the topographic correction. Based on the pre-exclusion and the SI, the mask of full shadow including self and cast shadow, can be mostly obtained through the binary segmentation method (Otsu, 1979).

3.1.2. The second pass: self shadow detection

In the topographic feature aspect, whether the slope is sun-facing or not can be determined by the solar position and the DEM. The solar elevation θ and azimuth ω are known. The slope angle α and aspect angle β of the surface are extracted from the DEM. Hence, the incidence angle i of an arbitrary pixel can be calculated by the following equation:

$$\cos i = \cos\alpha\cos\theta + \sin\alpha\sin\theta\cos(\beta - \omega) \tag{8}$$

It can be seen from Fig. 1 that the incidence angles of the shaded pixels (in self shadows) are large, corresponding to a small $\cos i$, while pixels on the sun-facing slopes have large $\cos i$ values. Based on the cosines of the incidence angles, we can obtain the distribution of the self shadows. Considering the detection errors in the above two passes, the intersection of the two detection results is determined as the self shadows.

Once the full shadows and self shadows are detected, the cast shadows can be obtained by subtracting the self shadows from the full shadows.

3.2. Variational framework considering cast shadows (CSVF)

As introduced before, most of the TC models are constructed on the basic assumption that the observed radiance L_T is positively related to the cosine of the incidence angle cos *i*as expressed by Eq. (3).

Cast shadows violate this basic linear assumption, due to the low L_T but high cos *i*. This is the reason why cast shadows cannot be corrected by the traditional TC methods. To solve the cast shadow problem, we propose the virtual cosine of the incidence angle ($\cos i_V$) to replace the original cos *i*. For the whole image, the $\cos i_V$ satisfies the linear relationship expressed by Eq. (3). To obtain the globally continuous and smooth $\cos i_V$, the variational framework is constructed, for which the solution can be optimized by numerical optimization iteration (Oliveira et al., 2009). Specifically, the $\cos i_V$ is composed of two parts: the $\cos i_V$ of non-cast shadows and the $\cos i_V$ of cast shadows.

For the non-cast shadows, including self shadows and sunlit areas, the cos *i* complies with the linear relationship, which means that the $\cos i_V$ should be equal to the original cos *i*. Using the variable *u* to represent $\cos i_V$ in the variational function, the constraint on non-cast shadows can be expressed as:

$$\int \|M_1(u - \cos i)\|_2^2 \tag{9}$$

where M_1 is the mark denoting the locations of non-cast shadows. This item constrains the closeness of the result to the original cos *i*.

For self shadows, the original cos *i* should be modified according to the linear relationship. Thus, the constraint item is constructed as follows:

$$\|M_2(bu + a - L_T)\|_2^2 \tag{10}$$

where M_2 is the matrix denoting the locations of the self shadow pixels, and *b* and *a* are the regression parameters calculated from the observed image. This item adjusts the incidence angles of self shadows by maintaining the linear relationship regressed by the non-self-shadow samples. Thus, the optimized $\hat{u}$ satisfies the linear relationship, for which the corresponding pixels can be corrected by the TC methods.

In addition to the above two items, the global constraint for the cosine of the incidence angle is constructed. The total variation prior is utilized, which can ensure the global spatial smoothness and maintain the local edge information, expressed as follows:

$$|\nabla u|_{TV} \tag{11}$$

Integrating the above three items, the variational model for optimizing the cosine of the incidence angle can be expressed as:

$$\hat{u} = \arg\min_u \frac{\alpha}{2}\|M_1(u - \cos i_0)\|_2^2 + |\nabla u|_{TV} + \frac{\beta}{2}\|M_2(bu + a - L_T)\|_2^2 \tag{12}$$

where α and β are the parameters used to weight the contributions of the corresponding items. This function can be solved by different numeric algorithms. Split Bregman iteration is used in this paper owing to its efficiency and stability (Goldstein and Osher, 2009). The solution of this function can be considered as the virtual cosine of the incidence angle, which can be used in the traditional TC models for the cast shadow correction.

3.3. Application of CSVF to the topographic correction (TC) models

The variational framework considering cast shadows (CSVF) can be generally applied to the current TC models. For simplification, all the correction methods considering cast shadows are named by the combination of CS and the original names, such as CS-C and CS-SEC. The C-correction is taken as an example to explain the application of CSVF.

As described in the second section, parameters *a* and *b* should be first estimated by the fitting of samples selected from the observed image. The estimation of these parameters should also be made in the CS-C correction. One point that should be noted is that the cast shadow pixels cannot be included in the selected samples, because they violate the linear relationship. Replacing the original $\cos i$ by the optimized virtual $\cos i_V$ in the C-correction model, the TC model considering cast shadows (CS-C) is constructed as shown in the following equation:

$$L_H = L_T \frac{\cos(sz) + c}{\cos i_V + c} \tag{13}$$

where $c = a/b$, and *a* and *b* are the regression parameters estimated by the non-cast-shadow samples. Actually, in the CS-C TC model, the cast shadows and self shadows are treated adaptively by considering their radiometric and topographic features. With the global constraint in the variational model, no artifacts are generated on the common boundary of cast and self shadows in the results. The other TC models considering cast shadows can be constructed in a similar way to CS-C.

4. Results and discussion

Landsat data of two mountainous regions were selected to test the proposed TC framework considering cast shadows. Considering the reasons for the appearance of cast shadows, mountains with high elevation differences were taken as the experimental regions. This scenario is difficult for the traditional TC methods to handle. The selected regions are located at Mount Yulong and the Wuyi Mountains of China. The observed DN data were transformed to TOA radiance by radiometric calibration, and dark object subtraction was used to remove the atmospheric disturbance. The DEM data were derived from ASTER GDEM v2 data with a 30-m. resolution. Registration between the radiance and DEM data was carried out before correction. The Yulong Mountains area is taken as an example to describe the cast shadow detection and restoration in detail. The results of three different TC methods for the two different regions are shown and compared. To evaluate the results quantitatively, the coefficients of determination were calculated.

4.1. Topographic correction of the Mount Yulong image

The image of Mount Yulong was acquired on 6 January 2002 by the Landsat ETM+ sensor, and the solar zenith is 56.32° and azimuth is 149.83°. The research area covers the west part of Yunnan province in China, with a 90 km × 90 km area, as shown in Fig. 2a. The registered DEM data with a 30-m resolution are shown in Fig. 2b. The main land-cover types of this area are forest, bare land, and water, and the water was screened out before shadow detection and correction.

4.1.1. Shadow detection

The shadows in the Mount Yulong image were detected based on the two passes using radiometric and topographic features. The detected full shadows, including self and cast shadows, are shown in Fig. 3, in which the self shadow pixels are rendered in blue and the cast shadow pixels in red. By visual assessment, most of the shadows in this image are detected, and the cast shadows appear along with the self shadows. When the self shadows and the shadow edges in the original image are compared, it can be seen that the locations of these two kinds of objects are consistent, which verifies the shadow detection precision. The execution time

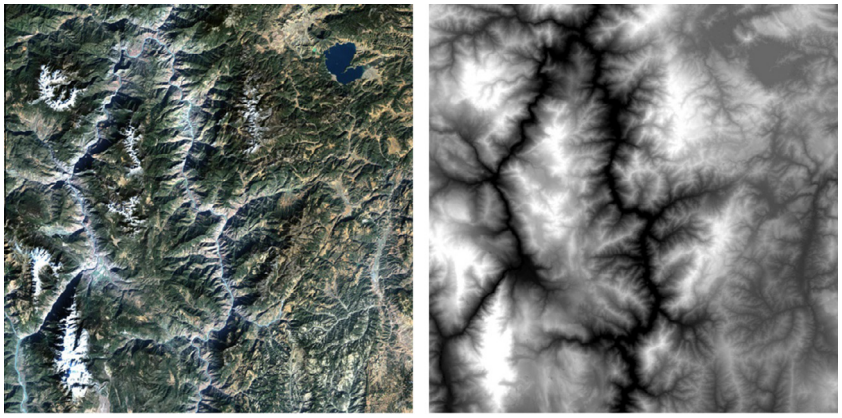

Fig. 2. Data of Mount Yulong. (a) ETM+ image composed of band 3, band 2, and band 1. (b) DEM.

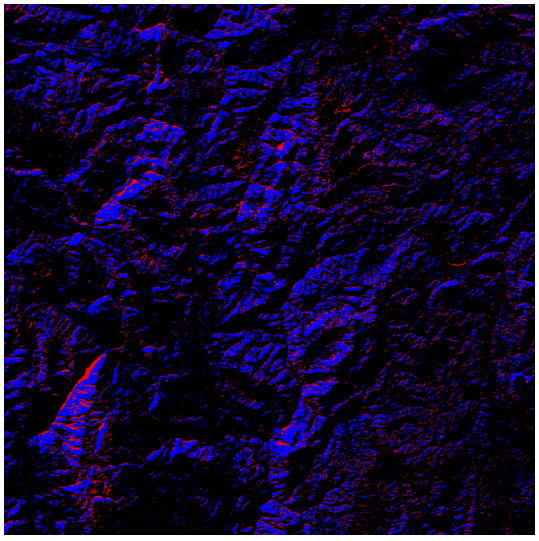

Fig. 3. The full shadows of the Mount Yulong image, including the self shadows in blue and the cast shadows in red. (For interpretation of the references to color in this figure legend, the reader is referred to the web version of this article.)

of the optimization is 471 s for the image with 3000 × 3000 pixels on a computer with an Intel CPU 2.4 GHz and 8G RAM.

As the self shadows can be precisely extracted by the topographic feature of the land surface, the cast shadow detection is mainly influenced by the radiometric feature based full shadow detection. To evaluate the detection result quantitatively, we clipped a sub-region from the original image, as shown in Fig. 4. The clipped image and DEM are shown in Fig. 4(a) and (b), and the detected self and cast shadows are shown in Fig. 4c and d. A full shadow mask was manually drawn and taken as a reference for the detection accuracy. The recall ratio A_R and precision ratio A_P were calculated to reflect the detection accuracy. The calculation formula can be expressed as the following two equations:

$$A_R = \frac{N_{dt}}{N_t} \times 100\% \tag{14}$$

$$A_P = \frac{N_{dt}}{N_d} \times 100\% \tag{15}$$

where N_{dt} represents the number of true shadow pixels in the detected shadows, N_t is the number of true shadow pixels, and N_d is the number of detected shadow pixels. The above indices respectively describe the ratios of the detection range and detection precision. For the results shown in Fig. 4c and d, the recall ratio and precision ratio are equal to 95.24% and 94.76%, which can satisfy our requirement in the shadow correction. This demonstrates the effectiveness and accuracy of the proposed detection method for remote sensing data.

4.1.2. Shadow correction

Once the self and cast shadow masks were obtained, the virtual cosines of the incidence angles for the whole image were optimized by the variational framework considering cast shadows (CSVF). The virtual cosines of the incidence angles were used in the three different TC models: C-correction, SCS, and SEC. The correction results for the Mount Yulong image are shown in the second column of Fig. 5. The first column of Fig. 5 shows the results of the original TC models.

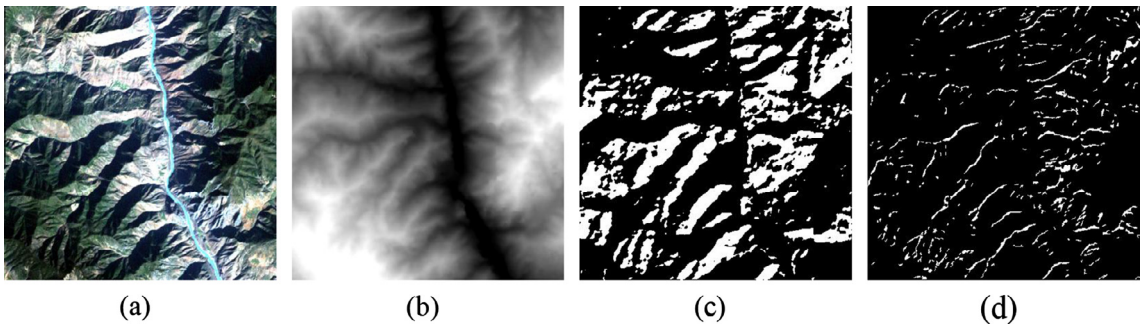

Fig. 4. Sub-region clipped from the Mount Yulong image. (a) Sub-image. (b) DEM. (c) Self shadows. (d) Cast shadows.

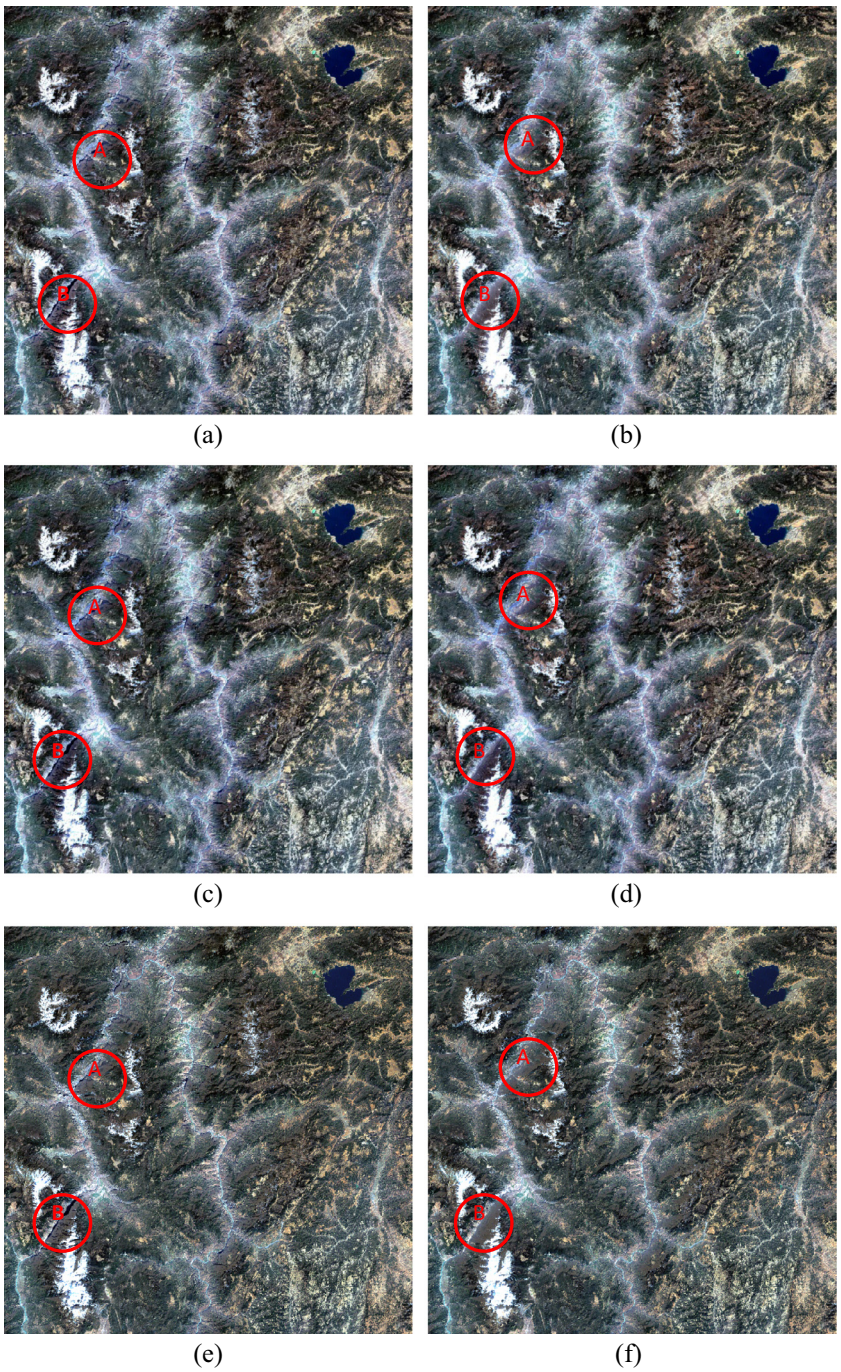

Fig. 5. The TC results of the traditional models and the models considering cast shadows. (a) C-correction result. (b) CS-C result. (c) SCS result. (d) CS-SCS result. (e) SEC result. (f) CS-SEC result.

Comparing the results of the original models and the models considering cast shadows, we can see that the latter results are flatter than the former. This is because the radiometric distortion caused by cast shadows is corrected in the results of the models considering cast shadows, but this is retained in the results of the original models. When examining the details, it can be found that the narrow dark strips in the left results are removed in the right results. Two regions, A and B, are clipped and enlarged and are shown in Figs. 6 and 7. Figs. 6a and 7a show the original images of the clipped regions, and the full shadows including self and cast shadows are shown in Figs. 6e and 7e. It can be seen that the proportion of cast shadows is too large to be neglected, which has an important influence on the TC results, as shown in the first row of Figs. 6 and 7. With the optimization of the incidence angles of the cast shadows in the models considering cast shadows, the results shown in the second row of Figs. 6 and 7 are better than the original results. The radiometric information of the cast shadow regions is compensated for, which improves the TC results and can benefit the application of remote sensing data.

For the quantitative assessment, the coefficients of determination were calculated. The coefficient of determination r^2 measures the linear relationship between the radiance and incidence angles in the results. The smaller the value of r^2, the less the relevance between the radiance and incidence angle, which means that the

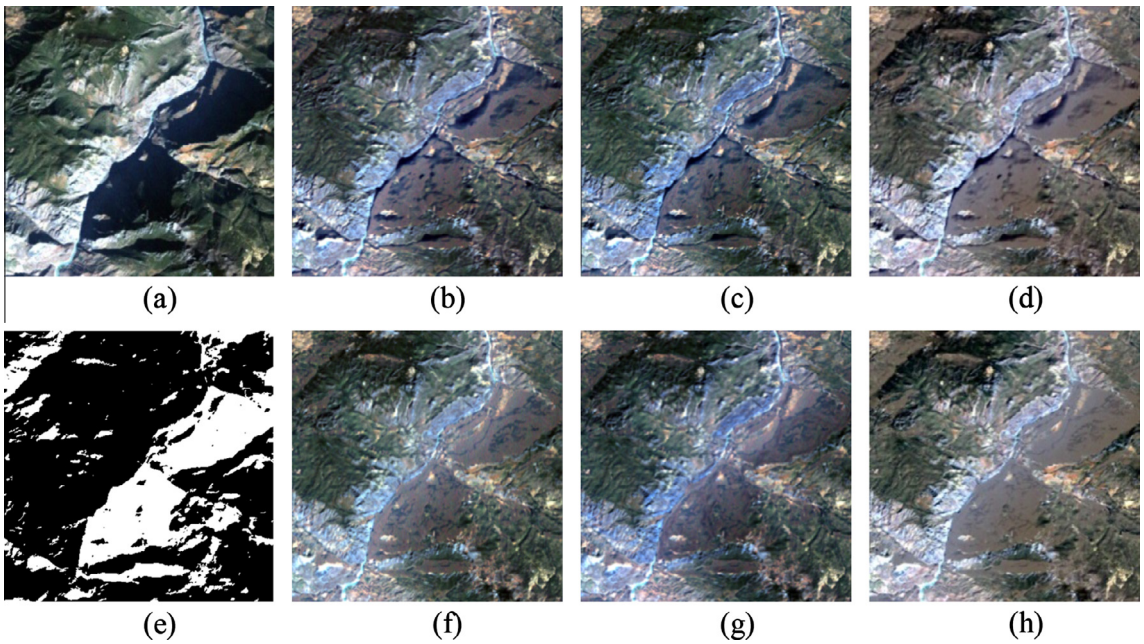

Fig. 6. The TC results of the first enlarged region from the Mount Yulong image. (a) Original image. (b)–(d) Results of C-correction, SCS, and SEC. (e) Full shadow in white including self and cast shadow. (f)–(h) Results of CS-C, CS-SCS, and CS-SEC.

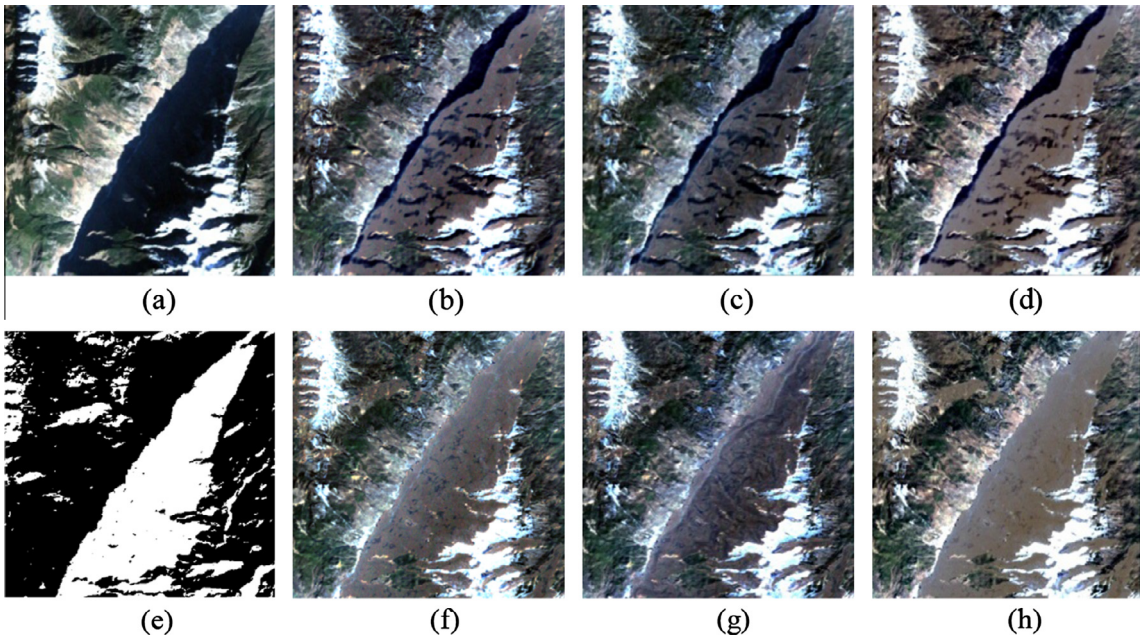

Fig. 7. The TC results of the second enlarged region from the Mount Yulong image. (a) Original image. (b)–(d) Results of C-correction, SCS, and SEC. (e) Full shadow in white including self and cast shadow. (f)–(h) Results of CS-C, CS-SCS, and CS-SEC.

TC is more effective. For the experiment with the Mount Yulong image, 100,000 samples were randomly selected from the image to calculate the coefficients of determination. This random process was repeated 10 times, and the average of the 10 results was recorded and used for the quantitative assessment. The coefficients for the original data and the different methods are listed in Table 1, where it can be clearly seen that the correction models considering cast shadows outperform the traditional models in all reflective bands, especially the infrared bands.

Table 1
The TC r^2 values for the Mount Yulong image.

	Band 1	Band 2	Band 3	Band 4	Band 5	Band 7
Original	0.1602	1.5130	7.8677	33.3077	307.7794	524.6475
C	0.0045	0.0330	0.1308	0.4226	0.6310	0.7520
CS-C	0.0042	0.0303	0.1191	0.3863	0.5332	0.6220
SCS	0.0067	0.0467	0.1790	0.4135	0.7557	0.9864
CS-SCS	0.0054	0.0353	0.1303	0.3201	0.4682	0.5823
SEC	0.0035	0.0166	0.0351	0.0743	0.0833	0.0689
CS-SEC	0.0027	0.0117	0.0234	0.0496	0.0509	0.0415

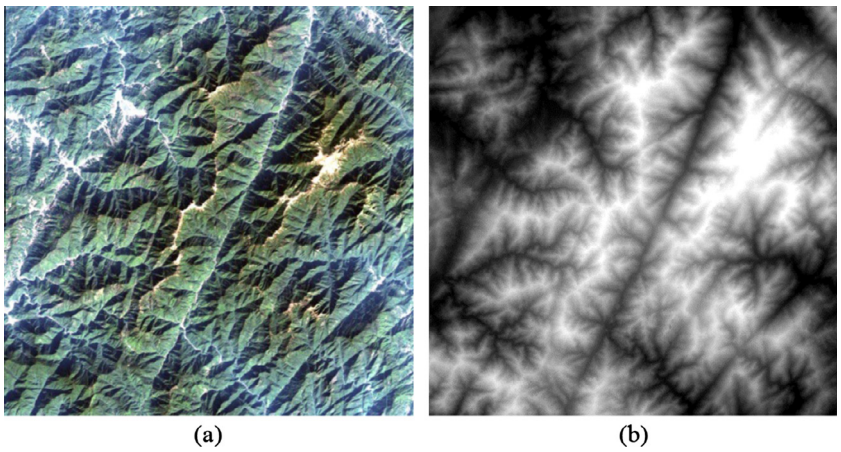

Fig. 8. The Wuyi Mountains data. (a) ETM+ image. (b) DEM.

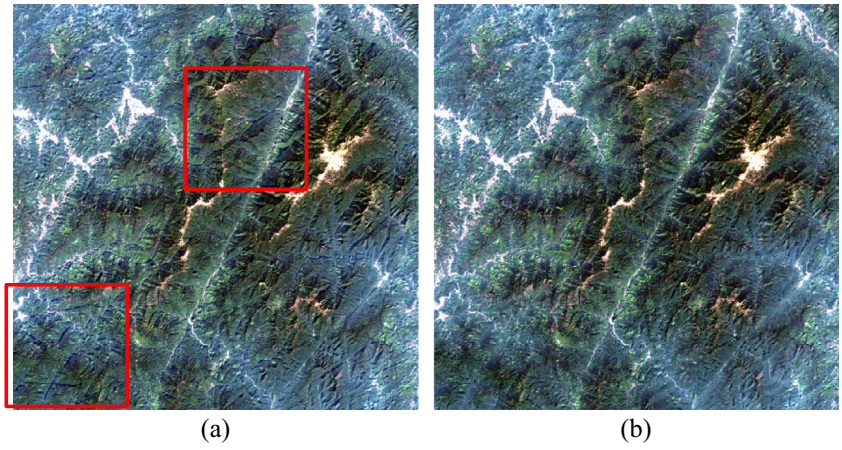

Fig. 9. The TC results of the Wuyi Mountains image. (a) The result of C-correction. (b) The result of CS-C.

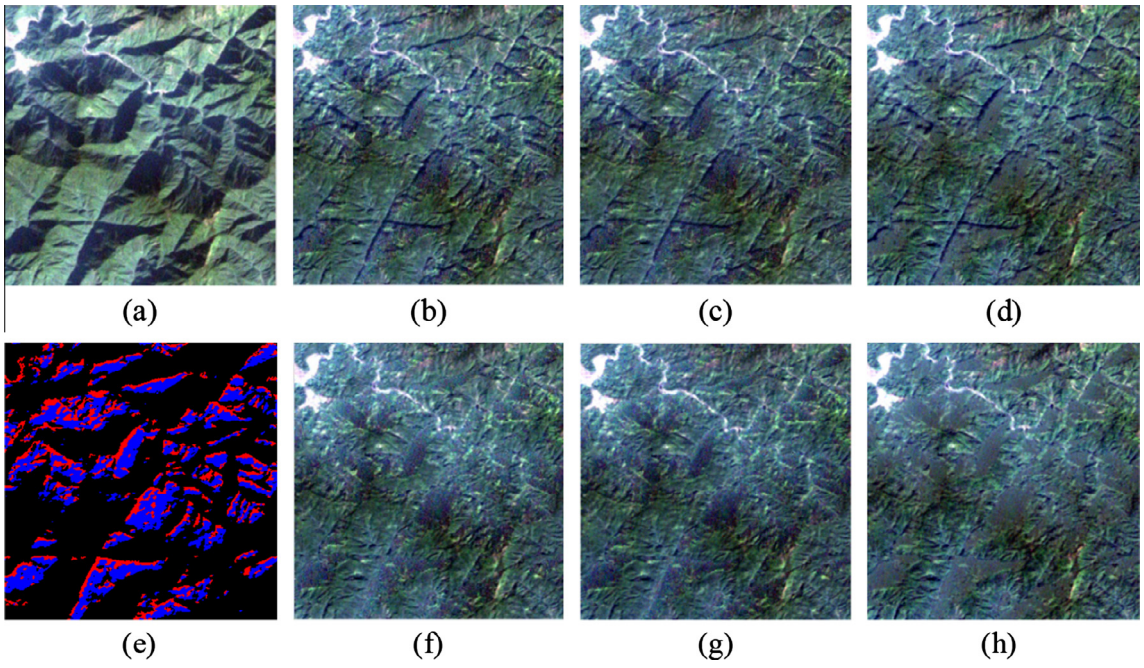

Fig. 10. The TC results of the first enlarged region from the Wuyi Mountains image. (a) Original image. (b)–(d) Results of C-correction, SCS, and SEC. (e) Shadows, including self shadows in blue and cast shadows in red. (f)–(h) Results of CS-C, CS-SCS, and CS-SEC. (For interpretation of the references to color in this figure legend, the reader is referred to the web version of this article.)

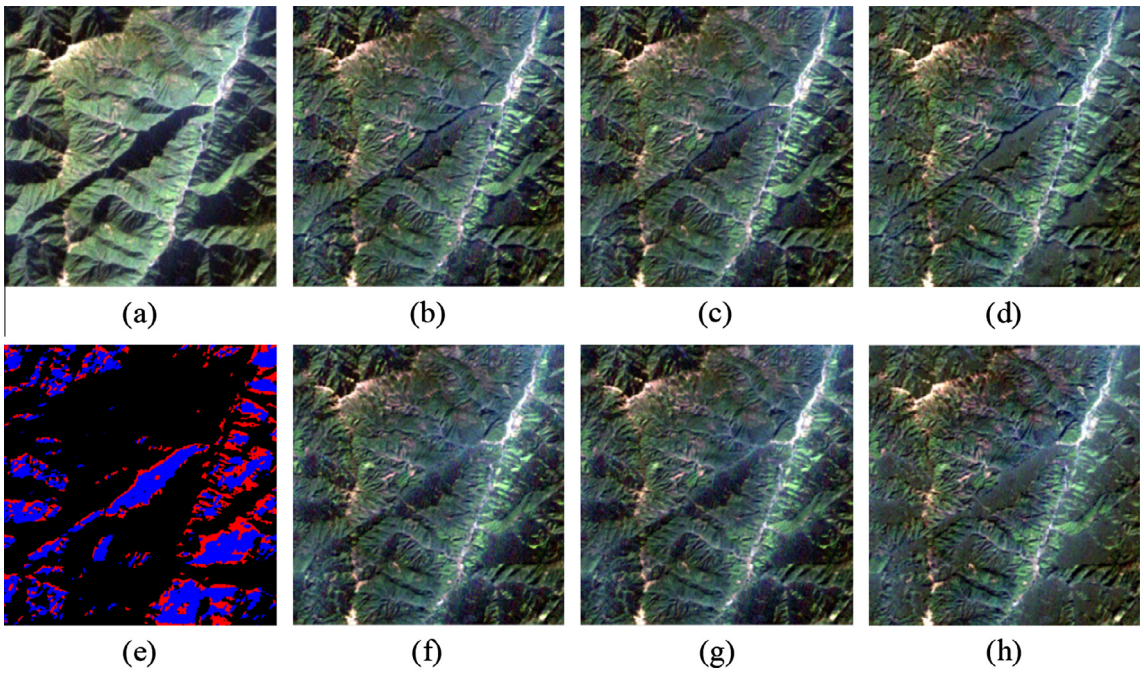

Fig. 11. The TC results of the second enlarged region from the Wuyi Mountains image. (a) Original image. (b)–(d) Results of C-correction, SCS, and SEC. (e) Shadows, including self shadows in blue and cast shadows in red. (f)–(h) Results of CS-C, CS-SCS, and CS-SEC. (For interpretation of the references to color in this figure legend, the reader is referred to the web version of this article.)

Table 2
The TC r^2 values for the Wuyi Mountains image.

	Band 1	Band 2	Band 3	Band 4	Band 5	Band 7
Original	0.5949	5.7084	3.8144	183.8376	195.0738	146.5018
C	0.0015	0.0056	0.0068	0.0524	0.0285	0.0321
CS-C	0.0002	0.0004	0.0010	0.0140	0.0037	0.0053
SCS	0.0028	0.0109	0.0120	0.0789	0.0499	0.0531
CS-SCS	0.0007	0.0020	0.0031	0.0256	0.0112	0.0130
SEC	0.0020	0.0034	0.0023	0.0292	0.0036	0.0001
CS-SEC	0.0006	0.0004	0.0001	0.0097	0.0001	0.0029

In addition to the differences between the results of the original models and the models considering cast shadows, the differences between the three models were also compared. From the color images composed of band 3, band 2, and band 1 shown in Fig. 5, it can be seen that the results of SEC are the flattest and the colors are more natural than the others. Quantitatively, the coefficients of determination for the results of the SEC models are the smallest, which is consistent with the visual assessment. This result is consistent with the result of a previous study analyzing TC methods (Hantson and Chuvieco, 2011).

4.2. Topographic correction of the Mount Wuyi image

In order to test the proposed variational framework further, another mountainous region was selected. The Landsat ETM+ image of the Mount Wuyi was acquired on 14 December 2001, covering an area of 30 km × 30 km, as shown in Fig. 8. The solar zenith

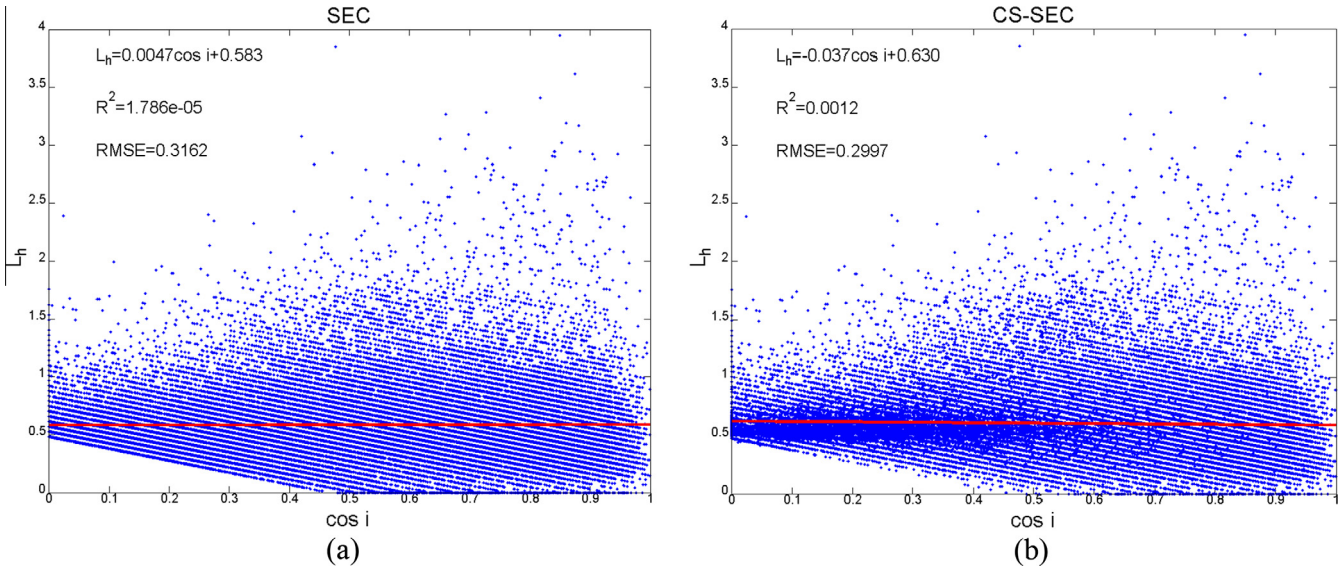

Fig. 12. Scatter plots of band 7. (a) Scatter plot of the 10 random samples for the result of SEC. (b) Scatter plot of the 10 random samples for the result of CS-SEC.

is 56.44° and the azimuth is 151.84°. The main land-cover type of this region is forest. The elevation ranges from 296 m to 2190 m, and the shadows caused by the topographic relief are obvious. The TC results of the different methods are shown in Fig. 9, and enlarged areas are shown in Figs. 10 and 11. As the scene is large, it is not easy to make a comparison from the whole image. Thus, Fig. 9 only shows one pair of results, i.e. the results of the C-correction and CS-C models, and the results of all the models for two clipped regions are enlarged and shown in Figs. 10 and 11. Visually, a similar conclusion can be made as for the Mount Yulong image, in that the cast shadows can be corrected by the models considering cast shadows, while they are uncorrected in the results of the original models.

Comparing the C-correction, SCS, and SEC models, it can be seen that the results of the SEC model are the flattest. This is because SEC is a kind of statistical information based mean approximation method, which is appropriate for homogeneous regions. The study areas, including both Mount Yulong and the Wuyi Mountains, are mainly covered by forest, which is homogeneous from the macroscopic view. Therefore, the results of the SEC and CS-SEC models are better than the other four models.

For the quantitative assessment, 50,000 samples were randomly selected from the image 10 times. The determination coefficients based on the random samples were calculated, and the average of each result is listed in Table 2. Compared with the traditional C-correction and SCS models, the CS-C and CS-SCS models raise the coefficients to a large degree for all bands. The coefficients of the CS-SEC result are larger than the SEC result in almost all the bands, except band 7.

To explore the difference between the SEC and CS-SEC results, we provide scatter plots of the results of the 10 random samples for band 7 in Fig. 12. The horizontal axis represents the cosines of the incidence angles, and the vertical axis represents the corrected radiance. The red line in the scatter plot is the regression line fitted by the samples. The large coefficient of determination for band 7 of the CS-SEC result can be attributed to the relatively large slope compared with that of the SEC result. However, we can see that the scatter plots in Fig. 12b are tighter to the mean radiance than those in Fig. 12a, which suggests the superiority of CS-SEC. On the other hand, the goodness of fit of the lines can also be considered, which can be described by the r^2 value and the root-mean-square error (RMSE). The larger the r^2 value or the smaller the RMSE, the better the linear fit. It can be seen that the r^2 value for the linear function in the SEC figure is 1.786e−05, i.e. very close to 0, which means that the fit of the line to the samples is poor. In contrast, the r^2 value for the CS-SEC result is 0.0012, which is larger than that of SEC. The RMSE of the SEC result is larger than that of CS-SEC. Integrating the coefficient of determination and the goodness of fit of the regression line, the superiority of CS-SEC for band 7 is still obvious.

5. Conclusions

A variational framework considering cast shadows (CSVF) has been proposed in this paper to improve the topographic correction (TC) of the current models. CSVF is a general framework which can be jointly used with the current TC models. It improves the TC results by correcting the radiometric distortion caused by cast shadows, which is neglected in the traditional TC models. The radiometric and topographic features are combined to detect self and cast shadows, respectively. The virtual cosines of the incidence angles can be generated by CSVF by imposing different constraints on the self and cast shadows, respectively. Three traditional TC models, C-correction, SCS, and SEC, were employed, and two different mountainous regions were selected to carry out the experiments. Both the visual and quantitative assessments verify the effectiveness of CSVF in correcting cast shadows and improving the TC results. The three traditional TC models were also compared in our experiments, where it was found that the SEC method performs well for the forest-dominated mountainous regions. The influence of the DEM resolution, precision and the surface cover variation on the cast shadow calculation and topographic correction accuracy will be investigated in our future work.

Acknowledgements

This work is supported by the National Natural Science Foundation of China (41401396) and National Science Fund for Distinguished Young Scholars of National Natural Science Foundation of China (41422108).

References

Balthazar, V., Vanacker, V., Lambin, E.F., 2012. Evaluation and parameterization of ATCOR3 topographic correction method for forest cover mapping in mountain areas. Int. J. Appl. Earth Obs. Geoinf. 18, 436–450.
Civco, D.L., 1989. Topographic normalization of Landsat Thematic Mapper digital imagery. Photogrammetric Eng. Remote Sens. 55 (9), 1303–1309.
Corripio, J., 2003. Vectorial algebra algorithms for calculating terrain parameters from DEMs and solar radiation modelling in mountainous terrain. Int. J. Geographical Inf. Sci. 17 (1), 1–23.
Dymond, J.R., Shepherd, J.D., Qi, J., 2001. A simple physical model of vegetation reflectance for standardising optical satellite imagery. Remote Sens. Environ. 75 (3), 350–359.
Fan, Y., Koukal, T., Weisberg, P.J., 2014. A sun–crown–sensor model and adapted C-correction logic for topographic correction of high resolution forest imagery. ISPRS J. Photogrammetry Remote Sens. 96, 94–105.
Funka-Lea, G., Bajcsy, R., 1995. Combining color and geometry for the active, visual recognition of shadows. In: Proceedings, IEEE Fifth International Conference on Computer Vision, pp. 203–209.
Gao, Y., Zhang, W., 2009. A simple empirical topographic correction method for ETM + imagery. Int. J. Remote Sens. 30 (9), 2259–2275.
Ge, H. et al., 2008. Pixel-based Minnaert correction method for reducing topographic effects on a Landsat 7 ETM+ image. Photogrammetric Eng. Remote Sens. 74 (11), 1343–1350.
Ghasemi, N., Mohammadzadeh, A., Sahebi, M.R., 2013. Assessment of different topographic correction methods in ALOS AVNIR-2 data over a forest area. Int. J. Digital Earth 6 (5), 504–520.
Goldstein, T., Osher, S., 2009. The split Bregman method for L1-regularized problems. SIAM J. Imaging Sci. 2 (2), 323–343.
Gu, D., Gillespie, A., 1998. Topographic normalization of Landsat TM images of forest based on subpixel sun–canopy–sensor geometry. Remote Sens. Environ. 64 (2), 166–175.
Hantson, S., Chuvieco, E., 2011. Evaluation of different topographic correction methods for Landsat imagery. Int. J. Appl. Earth Obs. Geoinf. 13 (5), 691–700.
Kaufman, Y., 1984. Atmospheric effects on remote sensing of surface reflectance. SPIE Proc. 475, 20–33.
Kobayashi, S., Sanga Ngoie, K., 2008. The integrated radiometric correction of optical remote sensing imageries. Int. J. Remote Sens. 29 (20), 5957–5985.
Kobayashi, S., Sanga Ngoie, K., 2009. A comparative study of radiometric correction methods for optical remote sensing imagery: the IRC vs. other image-based C-correction methods. Int. J. Remote Sens. 30 (2), 285–314.
Li, H., Zhang, L., Shen, H., 2014. An adaptive nonlocal regularized shadow removal method for aerial remote sensing images. IEEE Trans. Geosci. Remote Sens. 52 (1), 106–120.
McDonald, E.R., Wu, X., Caccetta, P.A., Campbell, N.A., 2002. Illumination Correction of Landsat TM Data in South East NSW. Environment Australia.
Meyer, P., Itten, K.I., Kellenberger, T., Sandmeier, S., Sandmeier, R., 1993. Radiometric corrections of topographically induced effects on Landsat TM data in an alpine environment. ISPRS J. Photogrammetry Remote Sens. 48 (4), 17–28.
Minnaert, M., 1941. The reciprocity principle in lunar photometry. Astrophys. J. 93, 403–410.
Oliveira, J.P., Bioucas-Dias, J.M., Figueiredo, M.A., 2009. Adaptive total variation image deblurring: a majorization–minimization approach. Signal Process. 89 (9), 1683–1693.
Otsu, N., 1979. A threshold selection method from gray-level histograms. IEEE Trans. Syst. Man Cybern. 9 (1), 62–66.
Proy, C., Tanre, D., Deschamps, P.Y., 1989. Evaluation of topographic effects in remotely sensed data. Remote Sens. Environ. 30 (1), 21–32.
Riaño, D., Chuvieco, E., Salas, J., Aguado, I., 2003. Assessment of different topographic corrections in Landsat-TM data for mapping vegetation types (2003). IEEE Trans. Geosci. Remote Sens. 41 (5), 1056–1061.
Richter, R., 1996. Atmospheric correction of satellite data with haze removal including a haze/clear transition region. Comput. Geosci. 22 (6), 675–681.

Richter, R., Kellenberger, T., Kaufmann, H., 2009. Comparison of topographic correction methods. Remote Sens. 1 (3), 184–196.
Sandmeier, S., Itten, K., 1997. A physically-based model to correct atmospheric and illumination effects in optical satellite data of rugged terrain. IEEE Trans. Geosci. Remote Sens. 35 (3), 708–717.
Smith, J.A., Lin, T.L., Ranson, K.L., 1980. The Lambertian assumption and Landsat data. Photogrammetric Eng. Remote Sens. 46 (9), 1183–1189.
Soenen, S., Peddle, D.R., Coburn, C., 2005. SCS+ C: a modified sun–canopy–sensor topographic correction in forested terrain. IEEE Trans. Geosci. Remote Sens. 43 (9), 2148–2159.
Teillet, P.M., Guindon, B., Goodenough, D.G., 1982. On the slope-aspect correction of multispectral scanner data. Can. J. Remote Sens. 8 (2), 84–106.
Teillet, P.M., Staenz, K., William, D.J., 1997. Effects of spectral, spatial, and radiometric characteristics on remote sensing vegetation indices of forested regions. Remote Sens. Environ. 61 (1), 139–149.
Vanonckelen, S., Lhermitte, S., Van Rompaey, A., 2013. The effect of atmospheric and topographic correction methods on land cover classification accuracy. Int. J. Appl. Earth Obs. Geoinf. 24, 9–21.